DOI:10.1190/segam2021-3581711.1

Target-oriented time-lapse elastic full-waveform inversion assisted by deep learning with prior information

Yuanyuan Li[1], Andrey Bakulin[2], Philippe Nivlet[2], Robert Smith[2] and Tariq Alkhalifah[1]
1- King Abdullah University of Science and Technology (KAUST), 2- EXPEC ARC, Saudi Aramco.

Summary

Time-lapse (TL) monitoring of the elastic property changes in the reservoir of interest is important for optimizing the reservoir interpretation and development plan. Given that elastic full-waveform inversion (EFWI) provides quantitative estimations of the elastic properties (Vp and Vs), its application to time-lapse elastic data is of considerable interest. For practical applications in reservoir monitoring, we need EFWI to provide high-resolution reservoir information at a reasonable cost. Thus, we develop an elastic redatuming technique to provide the required virtual elastic data for a target-oriented inversion, thus improving the computational efficiency by focusing our full-band inversion on the target zone. To improve the inversion resolution, we combine the well information and seismic data in the proposed time-lapse inversion approach using a regularized objective function. To derive the required prior model, we train a deep neural network (DNN) to learn the connection between the seismic estimation and the facies interpreted from well logs. We then apply the trained network to the target inversion domain to predict a prior model. Given the prior model, we perform another time-lapse inversion. We fit the simulated data difference for the virtual survey to the redatumed one from the surface recording and fit the model changes to the predicted prior model. The numerical results demonstrate that the proposed method enables the recovery of the time-lapse changes effectively in the target zone by incorporating the learned model changes from well logs.

Introduction

Knowledge of time-lapse (TL) changes of the subsurface elastic properties is crucial for reservoir characterization and management, monitoring the injected fluids, and evaluating the storage of CO2 in a carbon capture and storage (CCS) process (Lumley, 2001; Chadwick et al., 2010). Elastic full waveform inversion (EFWI) has been applied to time-lapse seismic data and shown reasonable potential in describing these property changes with high resolution (Zhang and Huang, 2013; Raknes et al., 2015). EFWI is computationally intensive, especially for time-lapse applications, because repeated experiments are required to derive the property changes. The computational cost will increase exponentially with increasing frequency often needed to enrich high-resolution information because fine discretization is required to simulate the high-frequency wavefield in a stable manner. Also, time-lapse EFWI (TLEFWI) is a highly ill-posed problem, hampered by non-uniqueness, inherent in EFWI (Tarantola, 1984). The trade-off between the multiple parameters poses more challenges in solving this inverse problem (Vigh et al., 2014).

The target-oriented inversion approach has been developed to reduce the computational cost by focusing the inversion on a localized area (Ayeni and Biondi, 2010; Yuan et al., 2017; Biondi et al., 2018). Redatuming techniques retrieve a virtual dataset for the target-oriented inversion by projecting sources and receivers to a datum level, preferably just above the target area (Wapenaar and Fokkema, 2006; Guo and Alkhalifah, 2020; Li et al., 2020a). To retain sufficient wave information in the virtual dataset for interpreting the elastic properties, we exploit the multi-component data on the surface in our elastic redatuming, instead of only the PP reflections (Garg and Verschuur, 2020; Biondi and Barnier, 2020), and generate the multi-component virtual dataset at the datum (Li and Alkhalifah, 2021).

Prior information can be incorporated into the inversion through regularization to mitigate its ill-posedness. Considering the injection and production wells are often present in the target zone, well information can complement the resolution and illumination (Asnaashari et al., 2013; Zhang et al., 2018; Singh et al., 2018; Li et al., 2020c). The model information in the sparsely-sampled wells should be projected to the inversion region to provide a prior model for regularization of the inversion. Deep learning (DL; LeCun et al., 2015) can efficiently learn a statistical relationship between the input and output features in a data-driven manner. Zhang and Alkhalifah (2019) and Li et al. (2020b, 2020c) employed deep neural networks (DNNs) to build the proper statistical connection that converts seismic estimates to facies interpreted from well logs and derived a prior model that incorporates the well information.

In the proposed method, we develop elastic redatuming to provide a virtual dataset for a target-oriented time-lapse EFWI. We also incorporate the well information to constrain the inversion by using a DL-assisted regularization technique to mitigate the trade-off and improve the resolution. Numerical tests on the Marmousi2 model are used to demonstrate the performance of the proposed method.

Target-oriented TL-EFWI using a deep learning assisted regularization

Theory

Elastic Waveform Redatuming

We develop the waveform redatuming technique (Guo and Alkhalifah, 2020; Li et al., 2020a) for elastic data. The redatuming process is an inverse problem that predicts the virtual elastic dataset (Green's function) at the datum level using the recorded multi-component data and a prior estimate of the overburden model. We can retrieve the redatumed elastic data ($\mathbf{g^D}$) by solving the following optimization problem:

$$\min_{\mathbf{g^D}} J = \frac{1}{2}\sum_s \left\| \mathbf{u}(\mathbf{m}_o) + \mathbf{u^D}(\mathbf{m}_o, \mathbf{g^D}) - \mathbf{d} \right\|_2^2 , \quad (1)$$

where, $\mathbf{d}$ is the recorded multi-component data, $\mathbf{m}_o$ refers to the overburden model, $\mathbf{g^D}$ is the virtual elastic data (Green's function) at the datum level, $\mathbf{u}$ refers to the simulated elastic data using $\mathbf{m}_o$. The elastic data from the datum ($\mathbf{u^D}$) is generated by using the following datum-based modelling operator:

$$\mathbf{F}u_n^D(\mathbf{x}, \mathbf{x}_s, t) = \iint u_p(\mathbf{x}_{vs} - \mathbf{h}, \mathbf{x}_s, t) * g_n^D(\mathbf{x}_{vs} - \mathbf{h}, \mathbf{x}_{vs}, t)\delta(\mathbf{x} - \mathbf{x}_{vs} + \mathbf{h}) d\mathbf{h} d\mathbf{x}_{vs} , \quad (2)$$

where, $\mathbf{F}$ is the elastic wave modeling operator, $\mathbf{h}$ is the subsurface offset vector measured from the virtual source $\mathbf{x}_{vs}$, n refers to x- or z-component of the elastic wavefield. The upgoing wavefield (u_n^D) is excited by the secondary source, located at the datum level, given by the convolution of the downgoing pressure-component wavefield (u_p) with the Green's function (g_n^D).

The gradient of the objective function with respect to the redatumed elastic data ($\mathbf{g^D}$) is written as:

$$\frac{\partial J}{\partial \mathbf{g}_n^{\mathbf{D}}}(\mathbf{x}_{vs} + \mathbf{h}, \mathbf{x}_{vs}, t) = -\sum_s \left\langle u_p(\mathbf{x}_{vs}, \mathbf{x}_s, t), u_n^{\dagger}(\mathbf{x}_{vs} + \mathbf{h}, \mathbf{x}_s, t) \right\rangle_t , \quad (3)$$

where $u^{\dagger}$ represents the backward propagating wavefield from the adjoint source at the receivers. We can obtain the gradient for the z- and x-components of the redatumed elastic data ($\mathbf{g}_z^{\mathbf{D}}, \mathbf{g}_x^{\mathbf{D}}$) by cross-correlating the forward pressure-component wavefield and the backward z- and x-component wavefield, respectively, at the datum level, followed by a summation over the sources. We will apply this elastic redatuming algorithm to the time-lapse elastic data to prepare the corresponding virtual datasets for the subsequent target-oriented time-lapse EFWI.

Regularized TLEFWI assisted by deep learning

Once the base and monitor datasets of the time-lapse experiment are redatumed to the datum level, we then perform the double-difference elastic waveform inversion (DDWI; Zhang and Huang, 2013) to estimate the property changes in the target zone. The double-difference objective function is defined as:

$$J_d(\mathbf{m}) = \frac{1}{2}\left\| \mathbf{u}(\mathbf{m}) - \mathbf{u}(\mathbf{m}_{ibase}) - \delta\mathbf{d}_{virtual} \right\|_2^2 . \quad (4)$$

In the DDWI algorithm, we first invert for the baseline model ($\mathbf{m}_{ibase}$) by matching the virtual baseline data. Then, we update the monitor model starting from $\mathbf{m}_{ibase}$ by minimizing the double-difference objective function. The model updates are considered to be the time-lapse changes.

To incorporate the prior information from well logs, a regularization term is added to the objective function:

$$J(\mathbf{m}) = J_d(\mathbf{m}) + \beta J_m(\mathbf{m}) , \quad (5)$$

where,

$$J_m(\mathbf{m}) = \left\| \mathbf{W}_m \left(\mathbf{m} - \left(\mathbf{m}_{ibase} + \delta\mathbf{m}_{prior} \right) \right) \right\|_2^2 , \quad (6)$$

and β is a weighting parameter, $\mathbf{W}_m$ is a diagonal weighting matrix, $\delta\mathbf{m}_{prior}$ is a prior model for the property changes in the target zone, that incorporates the well information predict from deep learning.

We derive the prior model by mapping the seismic estimation for the time-lapse dataset to the interpreted facies from wells based on their statistical relationship predicted by a deep neural network (DNN). The architecture of this fully-connected neural network is shown in Figure 1. Taking a vector $\mathbf{a}_0$ as inputs, a general forward-propagation equation is written as $\mathbf{a}_l = g_l(\mathbf{W}_l\mathbf{a}_{l-1} + \mathbf{b}_l)$, where $\mathbf{W}_l$ and $\mathbf{b}_l$ represent the weighting matrix and the bias vector for the lth layer, respectively. The activation function g_l is used to induce nonlinearity in the DNN. Here, we exploit the rectified linear unit (Relu) functions and a softmax activation function for the hidden layers and the output layer, respectively. The softmax function admits a neural network output given by a probability distribution over facies, written as $(p_{1,\cdots}, p_{i,\cdots}, p_{nf})$.

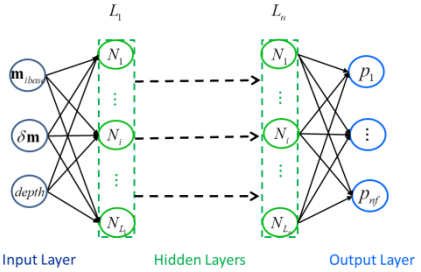

Figure 1: The architecture of the Deep Neural Network. There are four hidden layers and 64 neurons in each layer for the Marmousi2 example.

Both the inverted baseline model and the recovered velocity changes from seismic data serve as input features.

DOI:10.1190/segam2021-3581711.1

Considering the property changes often occur in a limited depth range, the depth of the training samples is also used as an input feature to improve the prediction accuracy of the DNN. We can interpret at least two facies, representing the injection and non-injection areas, from the wells to set labels for the training dataset. The injection area needs to be described by more than one facies in some complicated cases.

To improve the performance of the trained DNN, the Synthetic Minority Over-sampling Technique (SMOTE) is used to enlarge the training datasets and reduce the imbalance of different facies (Chawla et al., 2002). We also employ a random dropout of 30% to avoid over-fitting (Srivastava et al., 2014). Once the training process is finished, the DNN constructs a statistical connection between the inverted model's input features from the first EFWI and the facies classes. We then apply the trained network to the target inversion zone to predict the facies distribution. Considering that the velocity changes for each of the facies have been defined from the well logs, we can build the prior model for the velocity changes. Lastly, we implement a regularized TLEFWI by incorporating the prior model into the inversion.

Examples

We test the proposed inversion method on the modified Marmousi2 elastic model, shown in Figure 2, taken as the baseline model. Considering that the original Vs model needs very fine discretization to avoid dispersion, we reconstruct the Vs model based on a relationship of $V_s = V_p/\sqrt{3} + 0.1(V_p - 2.4)$. We implant velocity changes into the baseline model to build the monitor model. Figure 3 shows the time-lapse changes in the target zone, where Vp and Vs have changes of -200 m/s and -20 m/s, respectively. We design the datum level at a depth of 2.2 km, just above the monitoring zone.

We deploy 91 shots and 471 receivers evenly sampled at a depth of 20 m to generate the elastic multi-component data for the baseline and monitor models. The source wavelet is a Ricker wavelet with a peak frequency of 20 Hz. Starting from the initial model (Figure 4), we perform the conventional elastic FWI to estimate the baseline model using two low-frequency bands, 2-5 and 2-8 Hz, sequentially. Note that we only need set the spatial and time sampling intervals to 20 m and 2 ms for such frequency range, respectively. The inverted baseline Vp and Vs are shown in Figure 5. We then discretize the inverted model using a finer grid (5m) to handle the full-band simulation needed for the redatuming. Given the overburden model, we apply the elastic redatuming scheme to the recorded full-band baseline and monitor data to retrieve the corresponding virtual data. The virtual survey includes 58 virtual shots evenly sampled from 4 to 8.56 km at the datum level and 401 virtual receivers for each shot with a maximum offset of 1 km. Subtracting the baseline virtual data from the monitor virtual data, we obtain the time-lapse data difference for the virtual survey (Figure 6). The time-lapse Vp and Vs changes recovered from the target-oriented TLEFWI are shown in Figures 7a and 7b. We can see that the velocity changes are captured at the right position but still are contaminated by artifacts.

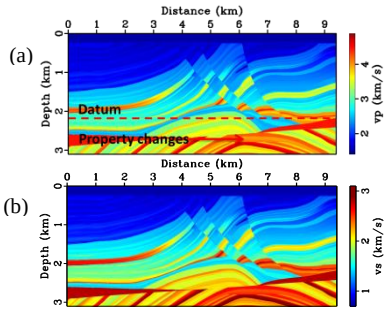

Figure 2: The true baseline (a) Vp and (b) Vs.

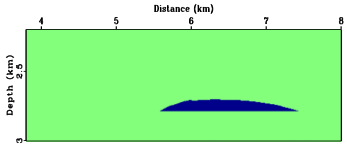

Figure 3: The true time-lapse changes in the target zone, where Vp and Vs has changes of -200m/s and -20m/s, respectively.

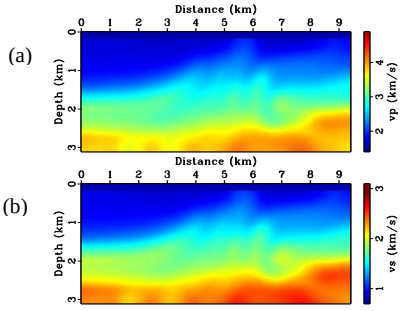

Figure 4: The initial (a) Vp and (b) Vs.

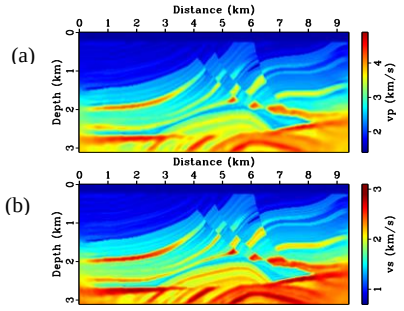

Figure 5: The inverted baseline (a) Vp and (b) Vs using conventional EFWI.

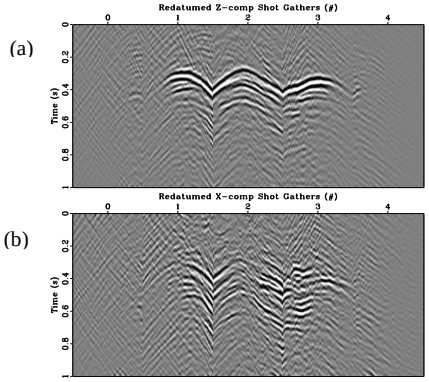

Figure 6: The time-lapse data difference for the virtual survey: (a) z-component and (b) x-component.

Two vertical profiles at 6.5 and 7.0 km are viewed as pseudo wells, which provide prior information of model changes to the target zone. We interpret two facies, representing the injection and non-injection areas, from these two wells to label the training dataset, which consists of the model samples near the well locations from the inverted model. Once the training is finished, the DNN learns a statistical relationship between the inverted model from time-lapse seismic data and the facies. Then, we apply the trained neural network to the target inversion zone to predict the facies distribution and derive the prior model for Vp and Vs changes (Figures 7c and 7d). At last, we conduct a regularized TLEFWI using the prior model. The recovered Vp and Vs changes, shown in Figures 7e and 7f, are better focused and cleaner than those without regularization (Figures 7a and 7b).

Conclusions

We introduce an elastic redatuming technique and deep-learning-assisted regularization to a time-lapse elastic full-waveform inversion scheme to improve the inversion performance. Elastic redatuming generates the virtual elastic dataset at the datum level for the target-oriented inversion, which reduces the computational cost by focusing the inversion on the target zone. The well logs, that provide detailed time-lapse property changes with limited coverage, complement the inversion resolution for seismic estimation using the proposed regularized inversion scheme. The required prior model is predicted from a trained deep neural network, which identifies the statistical connection between the seismic estimation and facies identified from well logs. The numerical example shows the potential of the proposed method in improving the inversion resolution and accuracy.

Acknowledgments

We want to thank the Shaheen supercomputing Laboratory in KAUST for their computational support. We thank KAUST and Saudi Aramco for the support and SWAG for a collaborative environment.

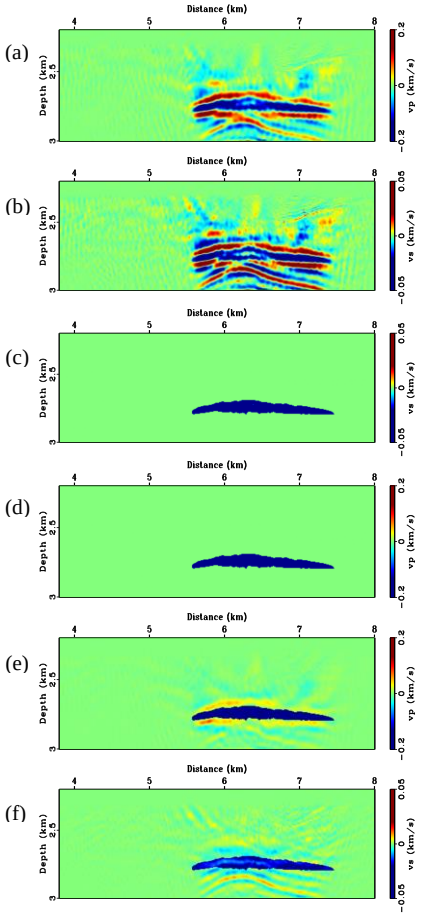

Figure 7: (a-b) The target-oriented TLEFWI result for Vp and Vs using the redatumed elastic data, (c-d) the predicted prior model for time-lapse Vp and Vs changes by using deep learning, (e-f) the final inverted Vp and Vs changes using the regularized inversion scheme.

REFERENCES

Asnaashari, A., R. Brossier, S. Garambois, F. Audebert, P. Thore, and J. Virieux, 2013, Regularized seismic full waveform inversion with prior model information: Geophysics, **78**, no. 2, R25–R36, doi: https://doi.org/10.1190/geo2012-0104.1.

Ayeni, G., and B. Biondi, 2010, Target-oriented joint least-squares migration/inversion of time-lapse seismic data sets: Geophysics, **75**, no. 3, R61–R73, doi: https://doi.org/10.1190/1.3427635.

Biondi, E., B. Biondi, and G. Barnier, 2018, Target-oriented elastic full-waveform inversion through extended-migration redatuming: 88th Annual International Meeting, SEG, Expanded Abstracts, 1228–1232, doi: https://doi.org/10.1190/segam2018-2998407.1.

Biondi, E., and G. Barnier, 2020, Elastic-parameter estimation by combining full-waveform inversion by model extension and target-oriented elastic inversion: 90th Annual International Meeting, SEG, Expanded Abstracts, 1–5, doi: https://doi.org/10.1190/segam2020-3428395.1.

Chadwick, A., G. Williams, N. Delepine, V. Clochard, K. Labat, S. Sturton, M. L. Buddensiek, M. Dillen, M. Nickel, A. L. Lima, and R. Arts, 2010, Quantitative analysis of time-lapse seismic monitoring data at the Sleipner CO_2 storage operation: The Leading Edge, **29**, 170–177, doi: https://doi.org/10.1190/1.3304820.

Chawla, N. V., K. W. Bowyer, L. O. Hall, and W. P. Kegelmeyer, 2002, SMOTE: Synthetic minority over-sampling technique: Journal of Artificial Intelligence Research, **16**, 321–357, doi: https://doi.org/10.1613/jair.953.

Garg, A., and D. J. Verschuur, 2020, From surface seismic data to reservoir elastic parameters using a full-wavefield redatuming approach: Geophysical Journal International, **221**, 115–128, doi: https://doi.org/10.1093/gji/ggz557.

Guo, Q., and T. Alkhalifah, 2020, Target-oriented waveform redatuming and high-resolution inversion: Role of the overburden: Geophysics, **85**, no. 6, R525–R536, doi: https://doi.org/10.1190/geo2019-0640.1.

LeCun, Y., Y. Bengio, and G. Hinton, 2015, Deep learning: Nature, **521**, 436–444, doi: https://doi.org/10.1038/nature14539.

Lumley, D. E., 2001, Time-lapse seismic reservoir monitoring: Geophysics, **66**, no. 1, 50–53, doi: https://doi.org/10.1190/1.1444921.

Li, Y., Q. Guo, T. Alkhalifah, and V. Kazei, 2020a, Target-oriented time-lapse waveform inversion using redatumed data: Feasibility and robustness: 90th Annual International Meeting, SEG, Expanded Abstracts, 1–5, doi: https://doi.org/10.1190/segam2020-3420515.1.

Li, Y., T. Alkhalifah, and Q. Guo, 2020b, Target-oriented time-lapse waveform inversion using a deep learning-assisted regularization: 90th Annual International Meeting, SEG, Expanded Abstracts, 1–5, doi: https://doi.org/10.1190/geo2020-0383.1.

Li, Y., T. Alkhalifah, and Z. Zhang, 2020c, High-resolution regularized elastic full waveform inversion assisted by deep learning: 82nd Annual International Meeting, EAGE, Expanded Abstracts, 1–5, doi: https://doi.org/10.3997/2214-4609.202010281.

Li, Y., and T. Alkhalifah, 2021, Target-oriented high-resolution elastic full waveform inversion using redatumed multi-component data: 82nd Annual International Meeting, EAGE, Expanded Abstracts, 1–5.

Raknes, E. B., W. Weibull, and B. Arntsen, 2015, Seismic imaging of the carbon dioxide gas cloud at Sleipner using 3D elastic time-lapse full waveform inversion: International Journal of Greenhouse Gas Control, **42**, 26–45, doi: https://doi.org/10.1016/j.ijggc.2015.07.021.

Singh, S., I. Tsvankin, and E. Z. Naeini, 2018, Bayesian framework for elastic full-waveform inversion with facies information: The Leading Edge, **37**, 924–931, doi: https://doi.org/10.1190/tle37120924.1.

Srivastava, N., G. Hinton, A. Krizhevsky, I. Sutskever, and R. Salakhutdinov, 2014, Dropout: A simple way to prevent neural networks from overfitting: The Journal of Machine Learning Research, **15**, 1929–1958.

Tarantola, A., 1984, Inversion of seismic reflection data in the acoustic approximation: Geophysics, **49**, no. 8, 1259–1266, doi: https://doi.org/10.1190/1.1441754.

Vigh, D., K. Jiao, D. Watts, and D. Sun, 2014, Elastic full-waveform inversion application using multicomponent measurements of seismic data collection: Geophysics, **79**, no. 2, R63–R77, doi: https://doi.org/10.1190/geo2013-0055.1.

Wapenaar, K., and J. Fokkema, 2006, Green's function representations for seismic interferometry: Geophysics, **71**, no. 4, SI33–SI46, doi: https://doi.org/10.1190/1.2213955.

Yuan, S., N. Fuji, S. Singh, and D. Borisov, 2017, Localized time-lapse elastic waveform inversion using wavefield injection and extrapolation: 2-D parametric studies: Geophysical Journal International, **209**, 1699–1717, doi: https://doi.org/10.1093/gji/ggx118.

Zhang, Z., and L. Huang, 2013, Double-difference elastic-waveform inversion with prior information for time-lapse monitoring: Geophysics, **78**, no. 6, R259–R273, doi: https://doi.org/10.1190/geo2012-0527.1.

Zhang, Z. D., T. Alkhalifah, E. Z. Naeini, and B. Sun, 2018, Multiparameter elastic full waveform inversion with facies-based constraints: Geophysical Journal International, **213**, 2112–2127, doi: https://doi.org/10.1093/gji/ggy113.

Zhang, Z., and T. Alkhalifah, 2019, Regularized elastic full waveform inversion using deep learning: Geophysics, **84**, no. 5, 1–47, doi: https://doi.org/10.1190/geo2018-0685.1.